ADVANCED FUNCTIONAL MATERIALS

Supporting Information

for *Adv. Funct. Mater.,* DOI: 10.1002/adfm.202204462

Lipid-Polymer Hybrid “Particle-in-Particle” Nanostructure Gene Delivery Platform Explored for Lyophilizable DNA and mRNA COVID-19 Vaccines

Zhongyu Li, Xue-Qing Zhang, William Ho, Xin Bai, Dabbu Kumar Jaijyan, Fengqiao Li, Ranjeet Kumar, Afsal Kolloli, Selvakumar Subbian, Hua Zhu, and Xiaoyang Xu**

Supporting Information

Lipid-polymer hybrid "Particle-in-Particle" nanostructure gene delivery platform explored for lyophilizable DNA and mRNA COVID-19 vaccines

Zhongyu Li, Xue-Qing Zhang, William Ho, Xin Bai, Dabbu Kumar Jaijyan, Fengqiao Li, Ranjeet Kumar, Afsal Kolloli, Selvakumar Subbian, Hua Zhu, and Xiaoyang Xu**

Z. Li, W. Ho, F. Li, X. Xu
Department of Chemical and Materials Engineering
New Jersey Institute of Technology
Newark, NJ 07102, USA
Email: xiaoyang.xu@njit.edu

X. Zhang, X. Bai
Engineering Research Center of Cell & Therapeutic Antibody Ministry of Education, School of Pharmacy
Shanghai Jiao Tong University
Shanghai 200240, P. R. China
E-mail: xueqingzhang@sjtu.edu.cn

D. Jaijyan, H. Zhu
Department of Microbiology, Biochemistry and Molecular Genetics
Rutgers—New Jersey Medical School
Newark, NJ 07103, USA

R. Kumar, A. Kolloli, S. Subbian,
Public Health Research Institute (PHRI)
Rutgers—New Jersey Medical School
Newark, NJ 07103, USA

X. Xu
Department of Biomedical Engineering

New Jersey Institute of Technology
Newark, NJ 07102, USA

	Mw (Dalton)	Mn (Dalton)	PDI (Mw/Mn)
PBAE-447	4173	2562	1.746
C12-PBAE (1:10)	5435	2892	1.879
C12-PBAE (1:5)	6241	3506	1.781
C12-PBAE (1:2)	8653	3626	2.386

Figure S1. Gel permeation chromatography (GPC) of C12-PBAE. The GPC results showed the molecular weight (MW) of C12-PBAE increased from 4173 Da to 5435, 6241, and 8653 Da with different molar ratios of C12-lipid to PBAE (from 1:10, 1:5 and 1:2) in the reactions, respectively. After calculating ΔMW/(MW of C12 lipid), there are an estimated six, twelve and twenty C12-lipids conjugated on the PBAE backbone, respectively.

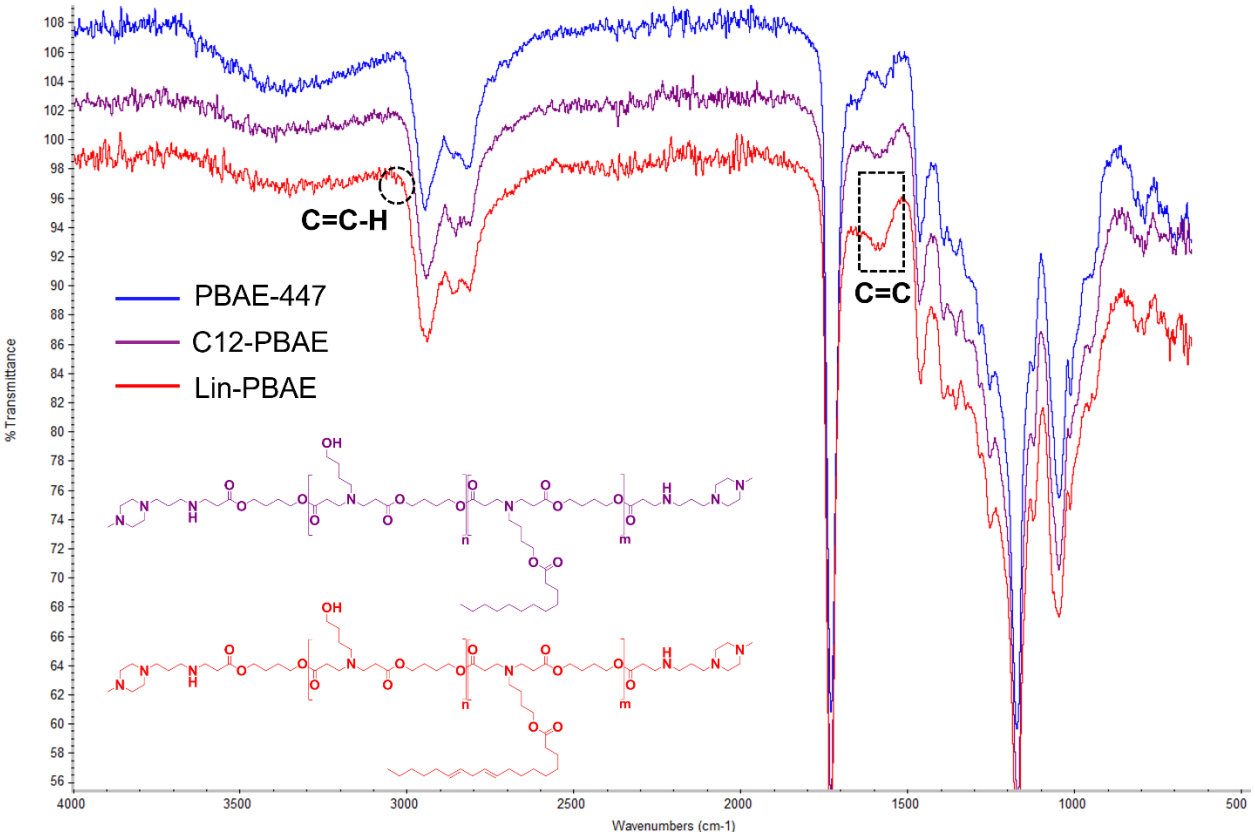

Figure S2. Fourier-transform infrared spectroscopy (FTIR) of L-PBAEs. The FTIR spectrum revealed the carbon-carbon double bond characteristic peaks of linoleic lipids conjugated on PBAE backbones. (C=C-H at ~3000 cm-1 and C=C at ~1600 cm-1)

A

PBAE-447

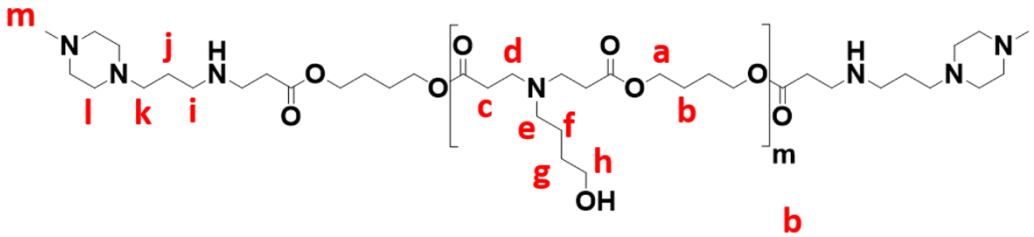
m
N
N
j
H
N
O
O
O
O
d
O
a
O
O
O
H
N
N
N
l
k
i
c
N
e
f
b
m
g
h
OH

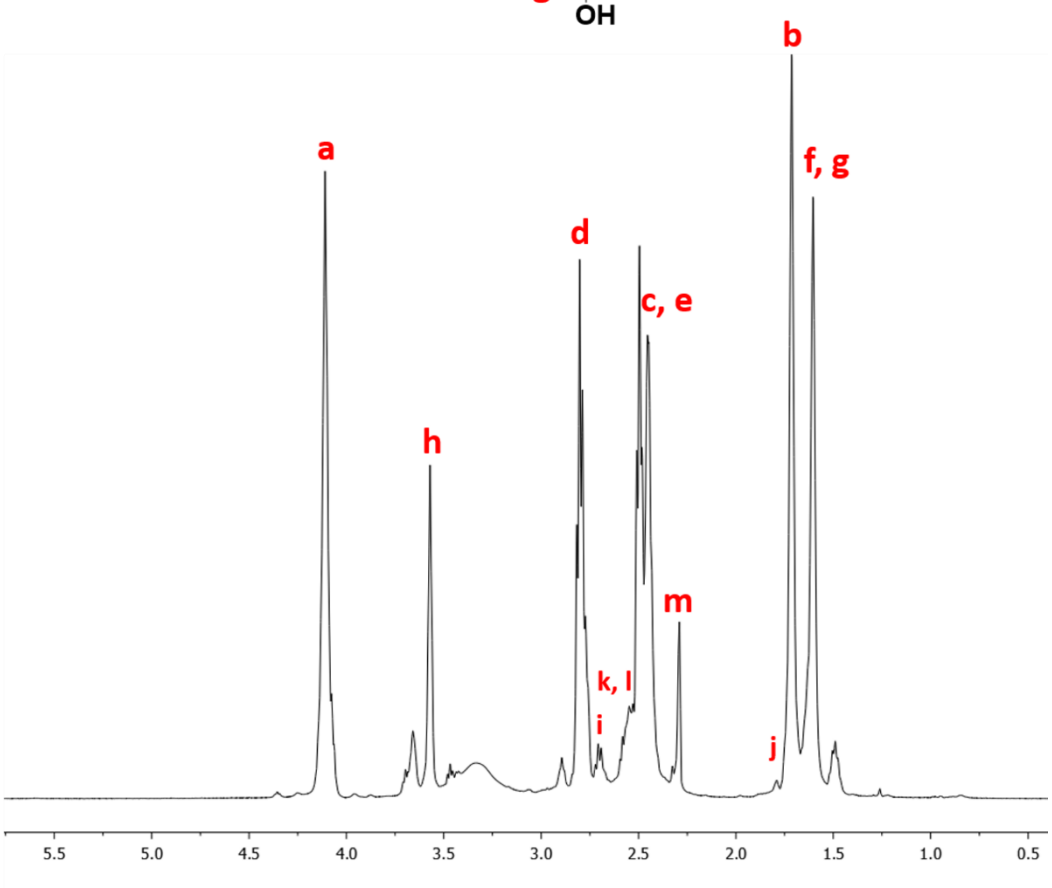
b
a
f, g
d
c, e
h
m
k, l
i
j
5.5
5.0
4.5
4.0
3.5
3.0
2.5
2.0
1.5
1.0
0.5

B

C12-PBAE

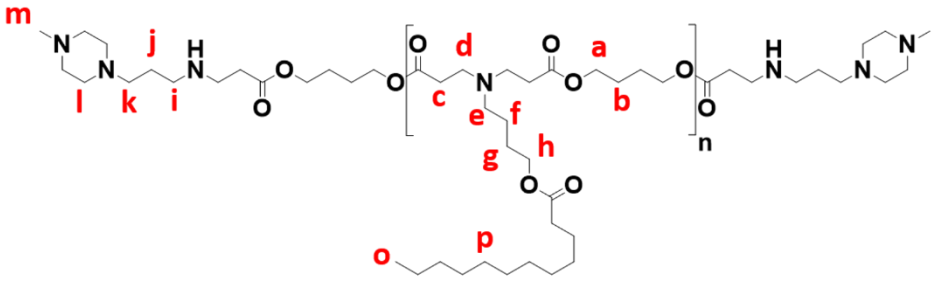
m
j
l
k
i
d
c
e
f
g
h
a
b
n
o
p

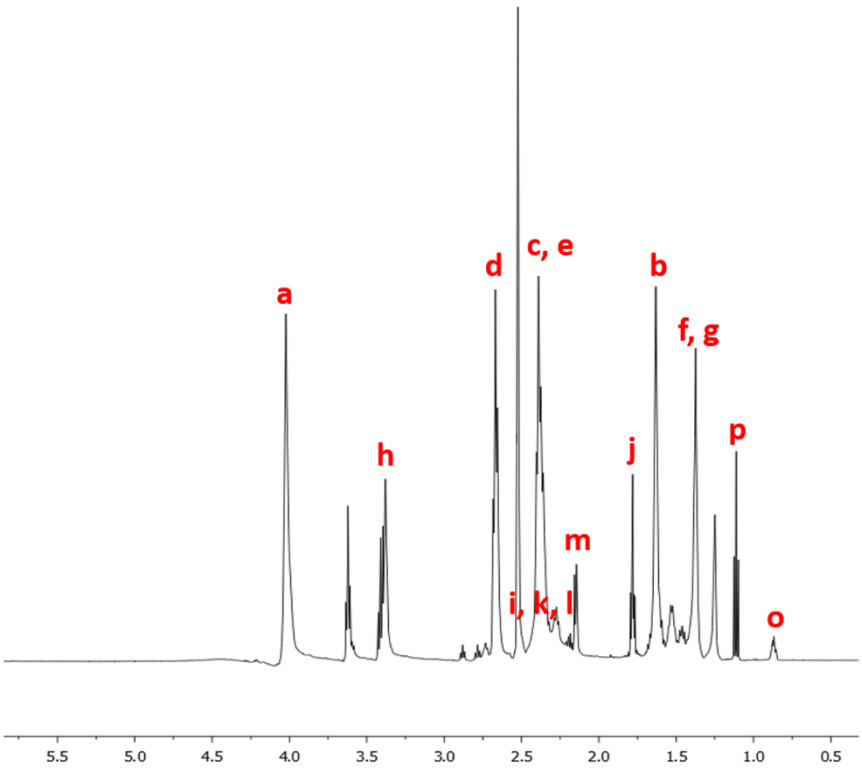
a
h
d
c, e
i, k, l
m
j
b
f, g
p
o
5.5
5.0
4.5
4.0
3.5
3.0
2.5
2.0
1.5
1.0
0.5

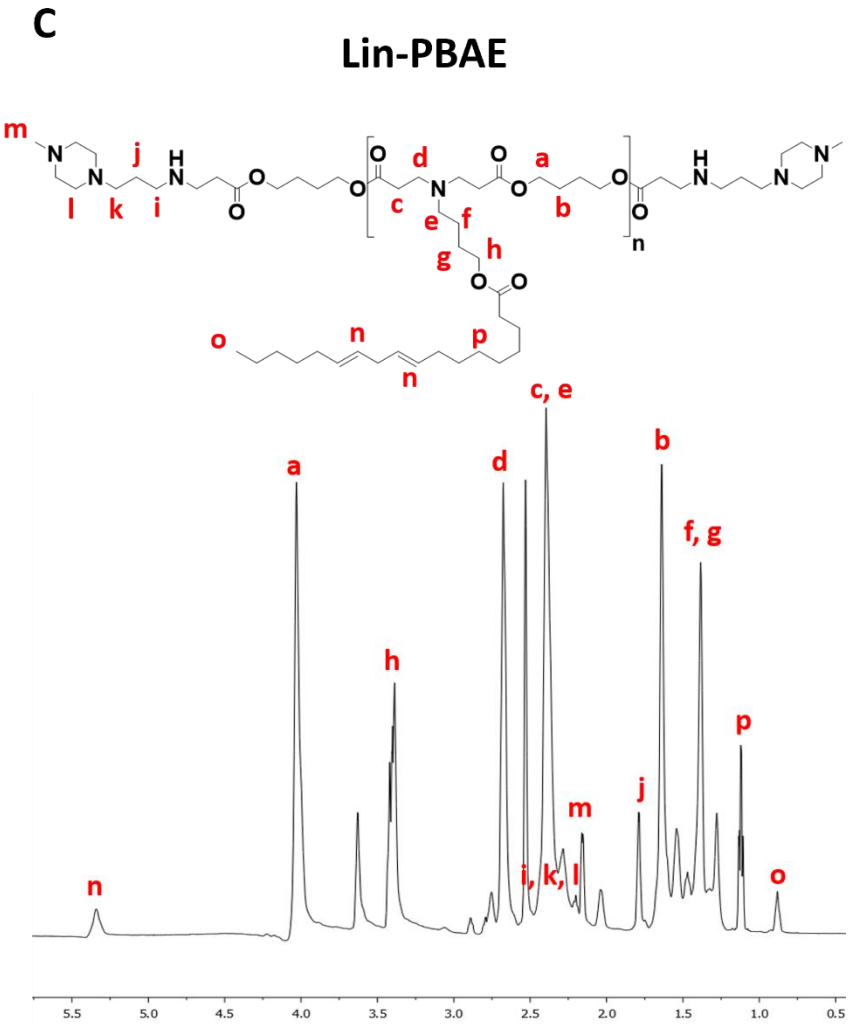

Figure S3. Nuclear Magnetic Resonance (NMR) spectroscopy of L-PBAEs. The conjugation of the C12-lipid and Linoleic-lipid on PBAE backbone were proved by NMR spectrum. The C12-lipid peaks of C12-PBAE were detected by NMR and briefly labeled 'o' and 'p' (**Figure S3B**) compared with the absence of these peaks in the original PBAE spectrum shown in **Figure S3A**. Similarly, the linoleic-lipid peaks of Lin-PBAE were also detected by NMR and labeled 'o', 'p' and 'n' (**Figure S3C**) which included carbon-carbon double bond characteristic peaks compared with C12-PBAE, which does not have an 'n' peak (**Figure S3B**).

Formulation	Size, nm	Polydispersity	Zeta potential, mV
PNP/C8-PBAE (1:10)	159.3	0.168	+26.3
PNP/C10-PBAE (1:10)	157.6	0.128	+28.8
PNP/C12-PBAE (1:10)	154.3	0.150	+26.8
PNP/C14-PBAE (1:10)	156.5	0.141	+27.1
PNP/C16-PBAE (1:10)	167.7	0.135	+26.5
PNP/C18-PBAE (1:10)	170.2	0.140	+25.1
PNP/Oleic-PBAE (1:10)	163.7	0.162	+22.3
PNP/Lin-PBAE (1:10)	161.6	0.154	+24.6
PNP/C12-PBAE (1:5)	178.5	0.175	+22.6
PNP/C12-PBAE (1:2)	209.2	0.171	+21.2
PNP/PBAE	175.5	0.158	+17.2

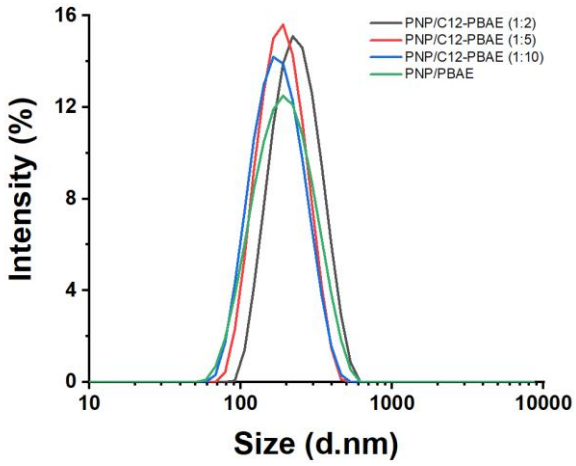

Figure S4. Characterization of different lipid molar ratios of PNP/L-PBAE NPs. Size distribution and zeta potential of PNP/L-PBAE NPs library were characterized. As the lipid molar ratios (of PBAE backbone) increased from 1:10 to 1:2, the NP size increased from 150 to 210 nm with narrow distribution of PDI of around 0.15.

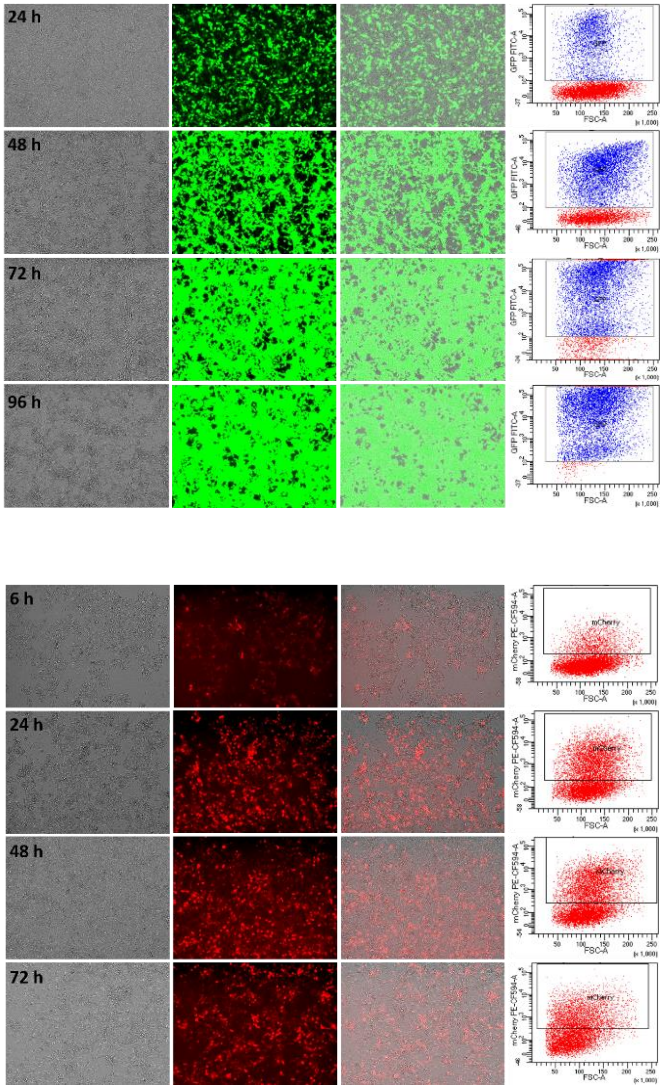

Figure S5. Characterization of long-term stored lyophilized PNP/C12-PBAE NPs. The lyophilized PNPs have been stored for 12 months at -20 °C and still maintained transfection efficacy for both plasmid (green) and mRNA (red) comparing to fresh PNPs. The comparison of size distribution of fresh and 12 months stored lyophilized PNP NPs.

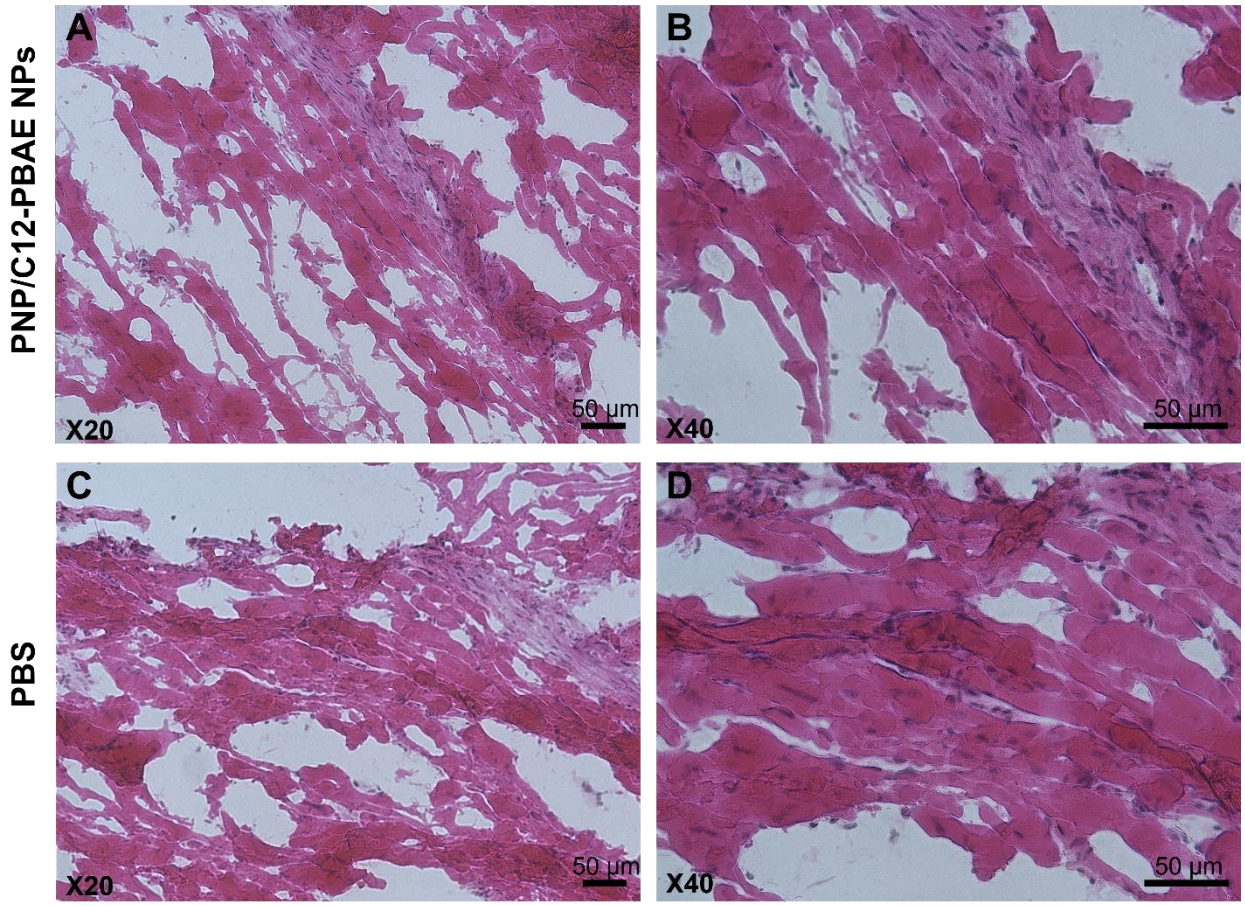

Figure S6. Histopathological analysis of muscle tissues surrounding nanoparticle injection site. (A) Muscle sections from mice in the PNP/C12-PBAE NP group were stained with haematoxylin and eosin (H&E), and representative photomicrographs were taken at 20x and (B) 40x magnification. (C) Muscle sections from the PBS group were stained with H&E and representative photomicrographs were taken at 20x and (D) 40x magnification (scale bars, 50 µm).

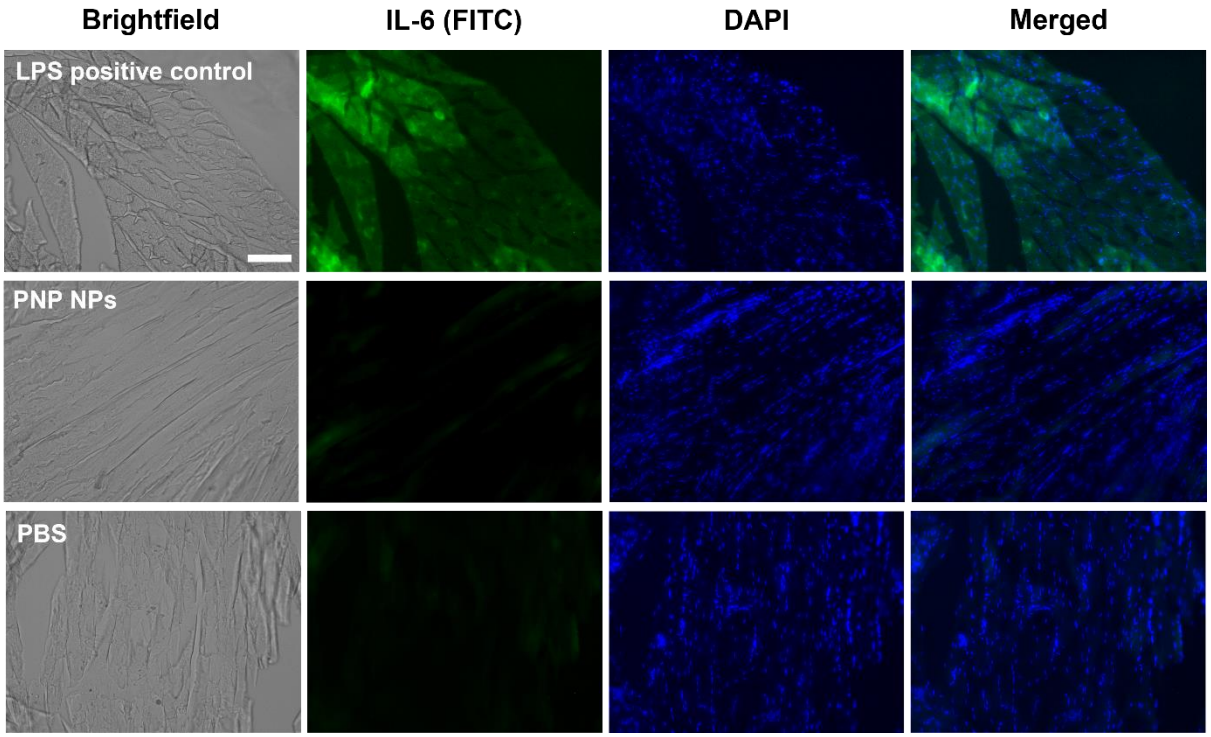

Figure S7. Immunofluorescence assay of IL-6 proinflammatory biomaker of muscle tissues surrounding nanoparticle injection site. Muscle sections from lipopolysaccharide LPS (1 μg/μL, 100 μL, top), PNP NPs (50 μL, middle) and PBS (50 μL, bottom) injected mice were detected by IL-6 antibodies, and representative photomicrographs were taken at 20x magnification under brightfield, FITC, DAPI and merged channels (scale bars, 50 μm).

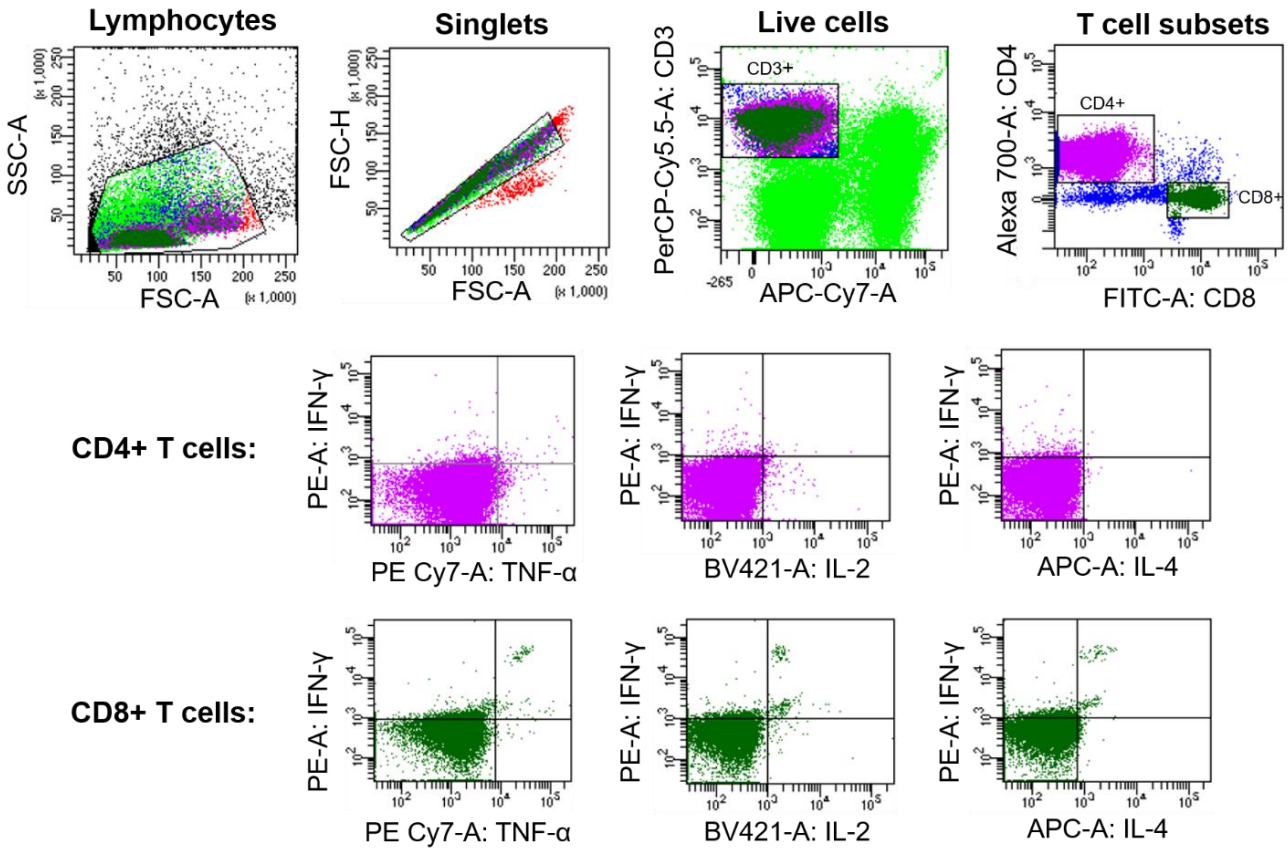

Figure S8. Flow cytometry gating strategy of intracellular cytokine staining. SARS-CoV-2 spike peptide pool stimulated T cells were stained and analyzed by flow cytometry. The T cell samples were gated to identify lymphocytes, singlets, live CD3+ T cells and T cell subsets of CD4+ and CD8+ T cells on the top row. For CD4+ and CD8+ T cells, the gates of IFN-γ, TNF-α, IL-2 and IL-4 were established (middle and bottom rows).

MFVFLVLLPLVSSQCVNLTTRTQLPPAYTNSFTRGVYYPDKVFRSSVLHSTQDLFLPF
FSNVTWFHAIHVSGTNGTKRFDNPVLPFNDGVYFASTEKSNIIRGWIFGTTLDSKTQS
LLIVNNATNVVIKVCEFQFCNDPFLGVYYHKNNKSWMESEFRVYSSANNCTFEYVSQ
PFLMDLEGKQGNFKNLREFVFKNIDGYFKIYSKHTPINLVRDLPQGFSALEPLVDLPIG
INITRFQTLLALHRSYLTPGDSSSGWTAGAAAYYVGYLQPRTFLLKYNENGTITDAVD
CALDPLSETKCTLKSFTVEKGIYQTSNFRVQPTESIVRFPNITNLCPFGEVFNATRFASV
YAWNRKRISNCVADYSVLYNSASFSTFKCYGVSPTKLNDLCFTNVYADSFVIRGDEV
RQIAPGQTGKIADYNYKLPDDFTGCVIAWNSNNLDSKVGGNYNYLYRLFRKSNLKPF
ERDISTEIYQAGSTPCNGVEGFNCYFPLQSYGFQPTNGVGYQPYRVVVLSFELLHAPA
TVCGPKKSTNLVKNKCVNFNFNGLTGTGVLTESNKKFLPFQQFGRDIADTTDAVRDP
QTLEILDITPCSFGGVSVITPGTNTSNQVAVLYQDVNCTEVPVAIHADQLTPTWRVYS
TGSNVFQTRAGCLIGAEHVNNSYECDIPIGAGICASYQTQTNSPRRARSVASQSIIAYT
MSLGAENSVAYSNNSIAIPTNFTISVTTEILPVSMTKTSVDCTMYICGDSTECSNLLLQ
YGSFCTQLNRALTGIAVEQDKNTQEVFAQVKQIYKTPPIKDFGGFNFSQILPDPSKPSK
RSFIEDLLFNKVTLADAGFIKQYGDCLGDIAARDLICAQKFNGLTVLPPLLTDEMIAQ
YTSALLAGTITSGWTFGAGAALQIPFAMQMAYRFNGIGVTQNVLYENQKLIANQFNS
AIGKIQDSLSSTASALGKLQDVVNQNAQALNTLVKQLSSNFGAISSVLNDILSRLDKV
EAEVQIDRLITGRLQSLQTYVTQQLIRAAEIRASANLAATKMSECVLGQSKRVDFCGK
GYHLMSFPQSAPHGVVFLHVTYVPAQEKNFTTAPAICHDGKAHFPREGVFVSNGTH
WFVTQRNFYEPQIITTDNTFVSGNCDVVIGIVNNTVYDPLQPELDSFKEELDKYFKNH
TSPDVDLGDISGINASVVNIQKEIDRLNEVAKNLNESLIDLQELGKYEQYIKWPWYIW
LGFIAGLIAIVMVTIMLCCMTSCCSCLKGCCSCGSCCKFDEDDSEPVLKGVKLHYT

Figure S9. Spike protein sequence. Amino acid sequence alignment of the full-length spike protein of SARS-CoV-2 used in PNP vaccine immunization studies.